MATERIALS CHEMISTRY
FRONTIERS

CHINESE CHEMICAL SOCIETY

ROYAL SOCIETY OF CHEMISTRY

RESEARCH ARTICLE

View Article Online
View Journal | View Issue

Cite this: *Mater. Chem. Front.*, 2022, **6**, 1647

Highly emissive and color-tunable copper-based halide composites for bright white light-emitting diodes†

Huanhuan Zhang,[a] Lin Yang,*[a] Hao Chen,[a] Wenqiang Ma,[a] Rui Wang[a] and Guozhong Cao*[b]

Lead-free metal halides have gained considerable attention due to their excellent optoelectronic properties; however, the direct synthesis of white light sources remains a challenge for developing high-performance white light-emitting diodes (WLEDs). Herein, we synthesized all-inorganic copper-based ternary halides using a microwave method. Through a strategy of controlling the amount of cuprous iodide (CuI), two highly efficient light emitters, blue-emissive $Cs_3Cu_2I_5$ and yellow-emissive $CsCu_2I_3$, can be obtained. The large Stokes-shifted broadband emission with a relatively long radiative lifetime is ascribed to the self-trapped exciton (STE) formation. The unique negative thermal quenching suggests that carrier transfer from more deeply trapped states to shallowly trapped states is beneficial for enhancing the STE emission. Moreover, with an increased amount of CuI, the as-synthesized $Cs_3Cu_2I_5$@$CsCu_2I_3$ composites exhibit a series of stable cold/warm white-light emissions. The bright WLEDs ranging from cold-white (12810 K) to pure-white (6109 K) and warm-white (4149 K) are displayed by placing the $Cs_3Cu_2I_5$@$CsCu_2I_3$ composite directly onto a commercial ultraviolet chip (310 nm), and an ultra-high color-rendering index (CRI) of 92 is achieved. The results imply that highly emissive and color-tunable copper-based halide composites open the door to explore their potential applications in next-generation solid-state lightings.

Received 25th February 2022,
Accepted 3rd May 2022

DOI: 10.1039/d2qm00172a

rsc.li/frontiers-materials

Introduction

In the past few years, lead-halide perovskites (LHPs) have made rapid progress and exhibited great potential in photoelectric devices due to their high color purity, tunable photoluminescence (PL) emission and high luminescence efficiency.[1–3] Significantly, the efficiency of LHP light-emitting diodes (LEDs) has been approaching those of the best performing organic LEDs.[4–6] However, the lead toxicity and poor stability of LHPs are two key issues in limiting the practical applications of devices.[7–9] To address these issues, many efforts have been devoted to explore the lead-free substitutions, including $CsSnI_3$,[10,11] $Cs_3Sb_2Br_9$,[12–14] $Cs_3Bi_2I_9$,[15] $Cs_3Cu_2I_5$,[16,17] $CsCu_2I_3$,[18,19] $Cs_2AgInCl_6$,[20] $Cs_2Zr_{1-x}Te_xCl_6$,[21] *etc.*

Among them, copper-based halides are termed as the low-cost, and environmentally friendly light emitters due to their bright luminescence, tunable emission wavelength and excellent stability.[22–24] Particularly, from the earlier studies, it can clarify that cesium copper halides have two crystal components on the basis of the different electronic structures, *i.e.*, $Cs_3Cu_2X_5$ and $CsCu_2X_3$ (X = Cl, Br, and I).[25,26] Taking Cu(I) halides for example, highly luminescent $Cs_3Cu_2I_5$ and $CsCu_2I_3$ display the blue and yellow broadband emissions, respectively, so they have been emerged as excellent sources for white-light generation.[27] Many synthesis methods have been used to prepare Cu(I) halides in recent years, such as hot injection,[16,28,29] antisolvent-assisted recrystallization,[30] solvent evaporation crystallization,[31] and so on. However, most of the methods require toxic organic solvents, posing environmental risks, and also enduring a very time-consuming and energy-consuming thermal path. More importantly, single-color Cu(I) halide is generally produced in an experiment with respect to the methods mentioned above. Using a hot-injection method, Vashishtha *et al.*[32] synthesized the blue-emissive (444 nm) $Cs_3Cu_2I_5$ and the yellow-emissive (561 nm) $CsCu_2I_3$, and they demonstrated the tunability of white-light emission with the Commission Internationale de l'Eclairage (CIE) coordinates from (0.145, 0.055) to (0.418, 0.541) by mixing the two compounds in different molar ratios. Grandhi *et al.*[33] also obtained

[a] College of Physics Science and Technology, Hebei University, Baoding 071002, Hebei, P. R. China. E-mail: yanglin@hbu.edu.cn; Fax: +86 312 5077069; Tel: +86 312 5077069
[b] Department of Materials and Engineering, University of Washington, Seattle, Washington 98195-2120, USA. E-mail: gzcao@u.washington.edu; Fax: +1 206 543 3100; Tel: +1 206 616 9084

† Electronic supplementary information (ESI) available. See DOI: https://doi.org/10.1039/d2qm00172a

the white-light emission by mixing $Cs_3Cu_2I_5$ and $CsCu_2I_3$ with a weight ratio of 1 : 16, and a reversible phase transformation between the two crystals was explored. However, the main drawback of the blended-ingredient strategy is that mixing multiple light emitters with a defined ratio would undoubtedly complicate the fabrication process of white LEDs (WLEDs) and yield the high cost. Another disadvantage of this strategy is that it would bring about a change in the white-light emission color over time owing to the unequal degradation rates of the light emitters and the efficiency losses owing to the self-absorption effect.[34] Most recently, Li *et al.*[35] prepared high-quality Cs–Cu–I nanoscale-thick films by thermal evaporation, and different proportions of phase structures corresponding to $CsCu_2I_3$ and $Cs_3Cu_2I_5$ were realized by adjusting the molar ratios of CsI and CuI powders. Ma and co-workers[36] synthesized $Cs_3Cu_2I_5$@-$CsCu_2I_3$ composites by a one-step solution method and demonstrated high-performance WLEDs with a high color-rendering index (CRI) of 91.6 and an excellent operation stability. Nevertheless, there are few prior reports pertaining to directly synthesizing the $Cs_3Cu_2I_5$@$CsCu_2I_3$ composite in the past few years.

This paper reports the synthesis of $Cs_3Cu_2I_5$@$CsCu_2I_3$ composites *via* a simple and facile microwave method for the first time. It is found that, with the increasing amount of cuprous iodide (CuI), the final products undergo a compositional evolution varying from the blue-emissive single-phase $Cs_3Cu_2I_5$ to the white-emissive composite $Cs_3Cu_2I_5$@$CsCu_2I_3$ and then to the yellow-emissive single-phase $CsCu_2I_3$. The subsequent optical characterization studies unravel that the remarkable emission of this series compound is assigned to self-trapped excitons (STEs) with the predominant features of large Stokes shift, broad spectrum and long lifetime, making it somewhat unusual as compared with other band-edge emissions in most of LHPs.[37,38] In view of the superior air stability of the samples, three cold/warm tunable WLEDs based on the $CsCu_2I_3$@$Cs_3Cu_2I_5$ composite were fabricated, and a CRI as high as 92 is obtained. Importantly, the synthesis method in this work can be extended to other copper-based ternary halides using different CuX (X = Cl, Br, and I) precursor salts. It would contribute to the development of nontoxic, air-stable and earth-abundant materials, which achieve an excellent opportunity for the light emitters, thereby resulting in a significant enhancement of high-performance WLEDs.

Experimental section

Chemicals

Cuprous iodide (CuI, 99.9%), cesium carbonate (Cs_2CO_3, 99.9%), oleylamine (OAm, 90.0%), oleic acid (OA, 90.0%), 1-octadecene (ODE, 90.0%) and polymethyl methacrylate (PMMA, $M_W \approx 550\,000$) were purchased from Aladdin. Methyl acetate ($C_3H_6O_2$, 98.0%) and toluene (C_7H_8, 99.5%) were obtained from Damao Chemical Reagent Factory. Hexane (C_6H_{14}, 99.5%) was obtained from Sinopharm Chemical Reagent Co., Ltd. All the chemicals were used as received without further purification.

Synthesis of Cs-oleate

Cs_2CO_3 (0.18 g) was loaded into a 20 mL glass bottle along with ODE (10 mL) and OA (0.6 mL), and the mixture was heated at 150 °C for 30 min until Cs_2CO_3 completely reacted with OA. The clear solution was continuously heated at 100 °C for further usage.

Synthesis of $Cs_3Cu_2I_5$, $Cs_3Cu_2I_5$@$CsCu_2I_3$ composites and $CsCu_2I_3$

In this work, CuI (1.3, 1.6, 1.7, 1.8 and 2 mmol), ODE (10 mL), OA (2 mL), OAm (2 mL) and 5 mL of Cs-oleate solution were loaded into a 35 mL quartz tube and then placed in a microwave reactor. The reaction mixture was maintained at 100 °C for 10 min, followed by cooling to room temperature naturally.

Centrifugation and purification of crude solutions

The solution was first centrifuged at 8000 rpm for 4 min, and then the precipitate was dispersed in 10 mL of hexane and centrifuged at 5000 rpm for 4 min. Afterward, the supernatant was mixed with 10 mL of methyl acetate and centrifuged at 8000 rpm for 4 min again. Finally, the precipitate was collected and air-dried.

Fabrication of WLED devices

PMMA was added into 3 mL of toluene and stirred at room temperature until a clear solution was obtained. Then, the composite powders were mixed in the solution, and finally, the mixture was coated on the surface of the ultraviolet LED chip (310 nm).

Characterization

The crystal structures of the as-prepared samples were measured using a X-ray diffractometer (XRD, BRUKER D8 ADVANCE) equipped with Cu Kα radiation. Transmission electron microscopy (TEM), the corresponding selected-area electron diffraction (SAED) and energy dispersive spectroscopy (EDS) elemental mapping were performed using a JEOL-2100 plus microscope. The morphologies of the products were examined using a scanning electron microscope (SEM, FEI Nova Nano SEM450). X-ray photoelectron spectra (XPS) were recorded using a Thermo SCIENTIFIC ESCALAB 250Xi spectrometer equipped with a monochromatic Al Kα radiation source ($h\nu$ = 1486.6 eV). Pass energies of 100 and 20 eV were used for survey and high-resolution scans, respectively, and the binding energies (BEs) were charge-corrected based on the C1s at 284.8 eV. Ultraviolet-visible (UV-vis) absorption spectra were recorded using a HITACHI U4100 UV-NIR spectrometer. Photoluminescence excitation (PLE) and photoluminescence (PL) spectra were recorded using a Hitachi F-7000 fluorescence spectrometer. Photoluminescence quantum yields (PLQYs) were recorded using a Hamamatsu Quantaurus-QY C11347-11 spectrometer. Time-resolved photoluminescence (TRPL) was performed using a Horiba Jobin Yvon Nanolog-TCSPC transient fluorescence spectrometer. Temperature-dependent PL spectra were measured using a Horiba Scientific Fluorolog-3 spectrometer. The chemical composition analysis was examined using a X-ray fluorescence spectrometer

(XRF, EDAX ORBIS). Electroluminescence (EL) spectra were recorded using an Ocean Optics USB 2000 spectrometer.

Results and discussion

$Cs_3Cu_2I_5$, $CsCu_2I_3$ and a series of $Cs_3Cu_2I_5$@$CsCu_2I_3$ composites were successfully synthesized by a microwave synthesis method, as schematically illustrated in Fig. 1(a). Here, ODE provides the solvent medium and OA/OAm act as the surface capping ligands. They are directly mixed with CuI and Cs-oleate and then placed in a microwave tube. The final products can be precisely controlled by changing the amount of CuI. Fig. 1(b) shows the XRD patterns of all samples with a whole range of 20–35°. The sample synthesized with 1.3 mmol CuI shows that the position and intensity of the diffraction peaks are in good agreement with those of the crystal planes of the orthorhombic $Cs_3Cu_2I_5$ (PDF#79-0333, space group *Pnma*). It is worth noting that the characteristic XRD patterns of the samples with 1.6, 1.7 and 1.8 mmol CuI exhibit two groups of diffraction peaks, which can be well indexed as orthorhombic $CsCu_2I_3$ and $Cs_3Cu_2I_5$, indicating that $Cs_3Cu_2I_5$@$CsCu_2I_3$ composites are obtained. When the amount of CuI is further increased to 2 mmol, the position and intensity of XRD are the same as those of the crystal planes of the orthorhombic $CsCu_2I_3$ (PDF#77-0069, space group Cmcm). Furthermore, the typical XPS spectra in Fig. S1 (ESI†) confirm the presence of Cs, Cu and I elements, and the two peaks located at ~932 and ~952 eV are assigned to Cu 2p with a valence of −1, which is consistent with the other reports.[33,39] As shown in the structure schematic (Fig. 1(c)), $Cs_3Cu_2I_5$ adopts a zero-dimensional (0D) structure, because $[Cu_2I_5]^{3-}$ species are separated from each other by Cs^+ ions, and each $[Cu_2I_5]^{3-}$ unit is composed of a $[CuI_4]^{3-}$ tetrahedron sharing an edge with a $[CuI_3]^{2-}$ triangle.[40] For $CsCu_2I_3$, the $[CuI_4]^{3-}$ tetrahedron share common edges, thus forming the double chains along the *c*-axis and becomes one-dimensional (1D) structure.[32]

The morphologies of samples were investigated by TEM and SEM characterization studies. The as-prepared $Cs_3Cu_2I_5$ and $CsCu_2I_3$ exhibit square and rod-like morphologies, as shown in

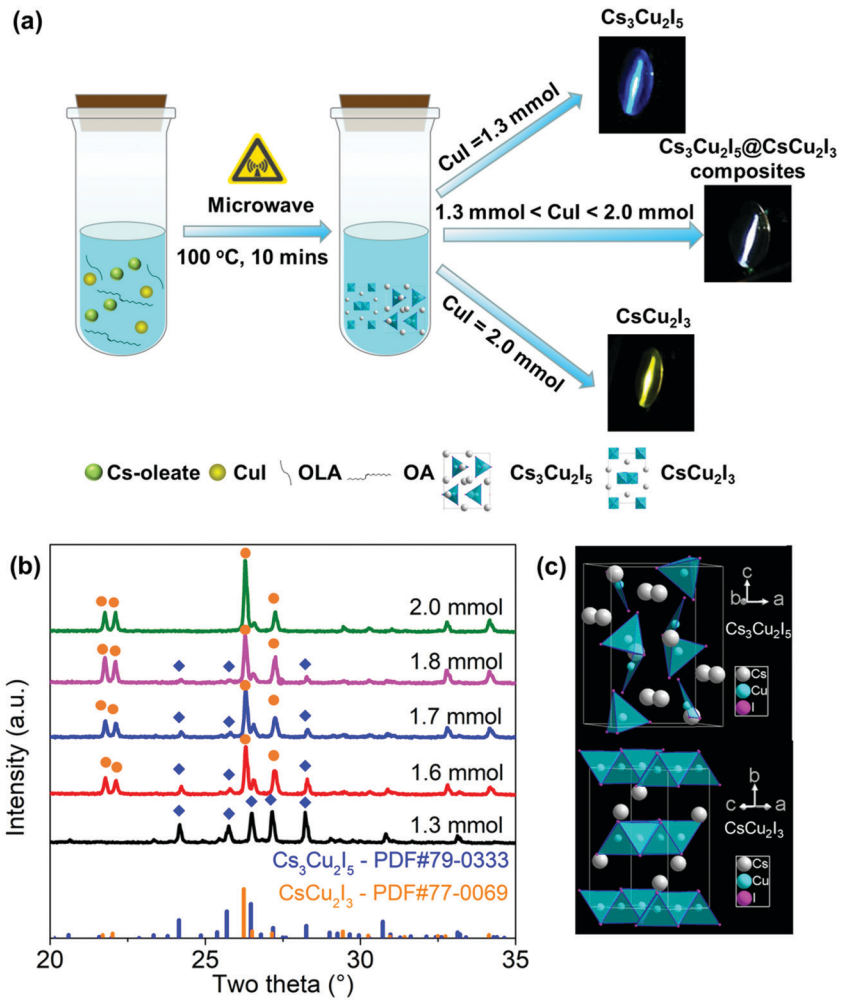

Fig. 1 (a) Schematic diagram of the microwave synthesis. (b) XRD patterns of samples synthesized with different amounts of CuI. (c) Crystal structures of $CsCu_2I_3$ and $Cs_3Cu_2I_5$.

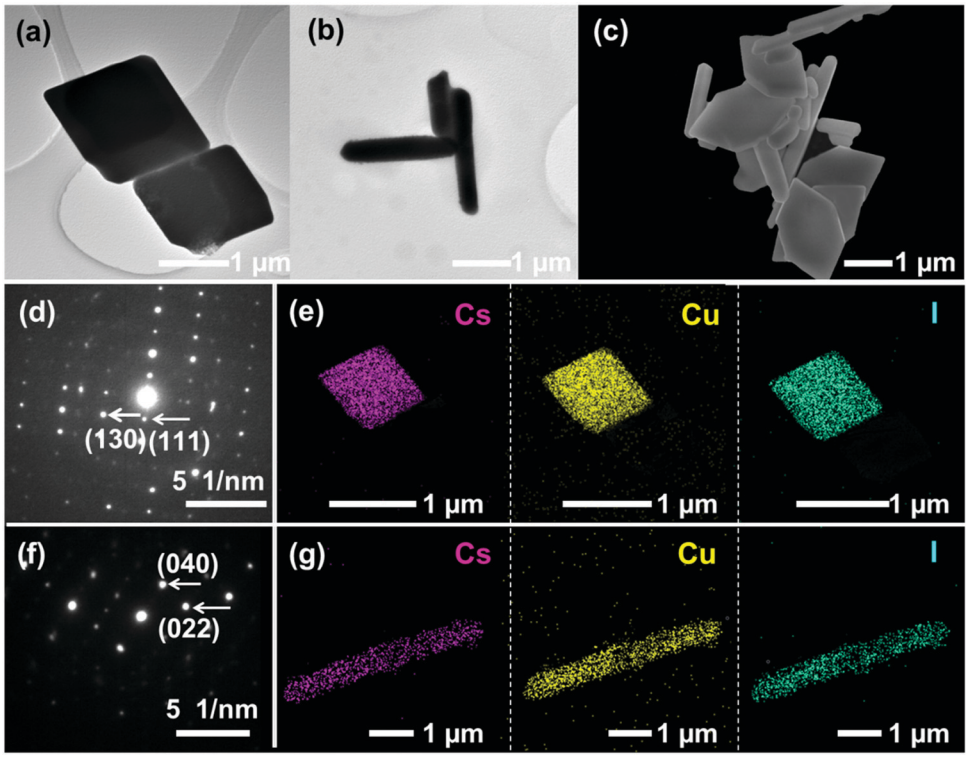

Fig. 2 TEM images of (a) $Cs_3Cu_2I_5$ and (b) $CsCu_2I_3$. (c) SEM image of $CsCu_2I_3$@$Cs_3Cu_2I_5$ composites. (d) SAED patterns of $Cs_3Cu_2I_5$. (e) EDS elemental mapping of Cs, Cu, and I elements in $Cs_3Cu_2I_5$. (f) SAED patterns of $CsCu_2I_3$. (g) EDS elemental mapping of Cs, Cu, and I elements in $CsCu_2I_3$.

Fig. 2(a) and (b), respectively. A SEM image of $Cs_3Cu_2I_5$@$CsCu_2I_3$ composites (Fig. 2(c)) demonstrates a morphological characteristic composed of hexagonal and rod-like shapes, indicating that the two ingredients, *i.e.*, $CsCu_2I_3$ and $Cs_3Cu_2I_5$, are coexisted in the composites without forming a compact structure. It is noted that the increased addition of CuI renders a morphology transformation of $Cs_3Cu_2I_5$ from square in the pure compounds to hexagonal in the composite, probably due to the alteration of facets' surface energy and growth kinetics with the high concentration of Cu. The corresponding SAED and EDS elemental mapping images of $Cs_3Cu_2I_5$ (Fig. 2(d) and (e)) and $CsCu_2I_3$ (Fig. 2(f) and (g)) confirm the high crystallinity without obvious defects and the uniform distributions of Cs, Cu, and I elements in the products.

Fig. 3(a) shows the UV-vis absorption spectra of $Cs_3Cu_2I_5$ and $CsCu_2I_3$ with absorption peaks at 275 and 325 nm, indicating band gaps of 4.35 and 3.70 eV (Fig. S3, ESI†), respectively, which are close to the values reported in the literature.[28,41] As we can see from the PLE and PL spectra in Fig. 3(b), $Cs_3Cu_2I_5$ exhibits a broad blue emission peak at 455 nm with a full width at half-maximum (FWHM) of 80 nm. The maximum peak in the PLE spectrum of $Cs_3Cu_2I_5$ is at 297 nm, and hence, the Stokes shift is 158 nm. Meanwhile, $CsCu_2I_3$ shows a broad emission peak at 580 nm (FWHM = 123 nm) with a large Stokes shift of 253 nm. The characteristics of a large Stokes shift and a broad peak width are ascribed to the STEs, which originate from the excited-state structural reorganization due to the local structural symmetry enhanced by the Jahn–Teller distortion of the $[CuI_4]^{3-}$ tetrahedra.[16] As depicted in Fig. 3(c) and (d), upon photoexcitation, electrons are excited from the ground state to the excited state and, simultaneously, an excited-state structural distortion takes place, which enables the formation of STEs. Therefore, the photoexcited electrons prefer to undergo an intersystem crossing to triplet STEs, consequently leading to the strongly Stokes-shifted broadband emission.

To obtain further information about the STE dynamics, the TRPL decay dynamics of $Cs_3Cu_2I_5$ and $CsCu_2I_3$ were measured and the results are shown in Fig. 3(e) and (f). The lifetimes of $Cs_3Cu_2I_5$ and $CsCu_2I_3$ are obtained as 1.56 and 7.03 μs, respectively, greatly superior to other previous studies on copper-based halides prepared by other methods.[26,40,41] Such long lifetimes of microseconds indicate the slow radiative decay of the STE emission. Moreover, $Cs_3Cu_2I_5$ has a higher PLQY of 50% than that of $CsCu_2I_3$ (PLQY = 9%), although the PL mechanism of these two materials is similar. This is generally due to the efficient self-trapping of photoexcited charge carriers in $Cs_3Cu_2I_5$. The low PLQY of $CsCu_2I_3$ can be ascribed to its lower self-trapping depth, corresponding to a higher detrapping rate of trapped excitons.[33] Furthermore, with regard to $Cs_3Cu_2I_5$, both PLE spectra monitored at different emission wavelengths (Fig. 4(a)) and PL spectra measured at different excitation wavelengths (Fig. 4(b)) show the identical features, respectively, demonstrating that the broad blue emission comes from the same excited state, which provides an evidence for the STE emission as well. $CsCu_2I_3$ has the same characteristics as shown in Fig. S2 (ESI†). The temperature-dependent PL spectra and

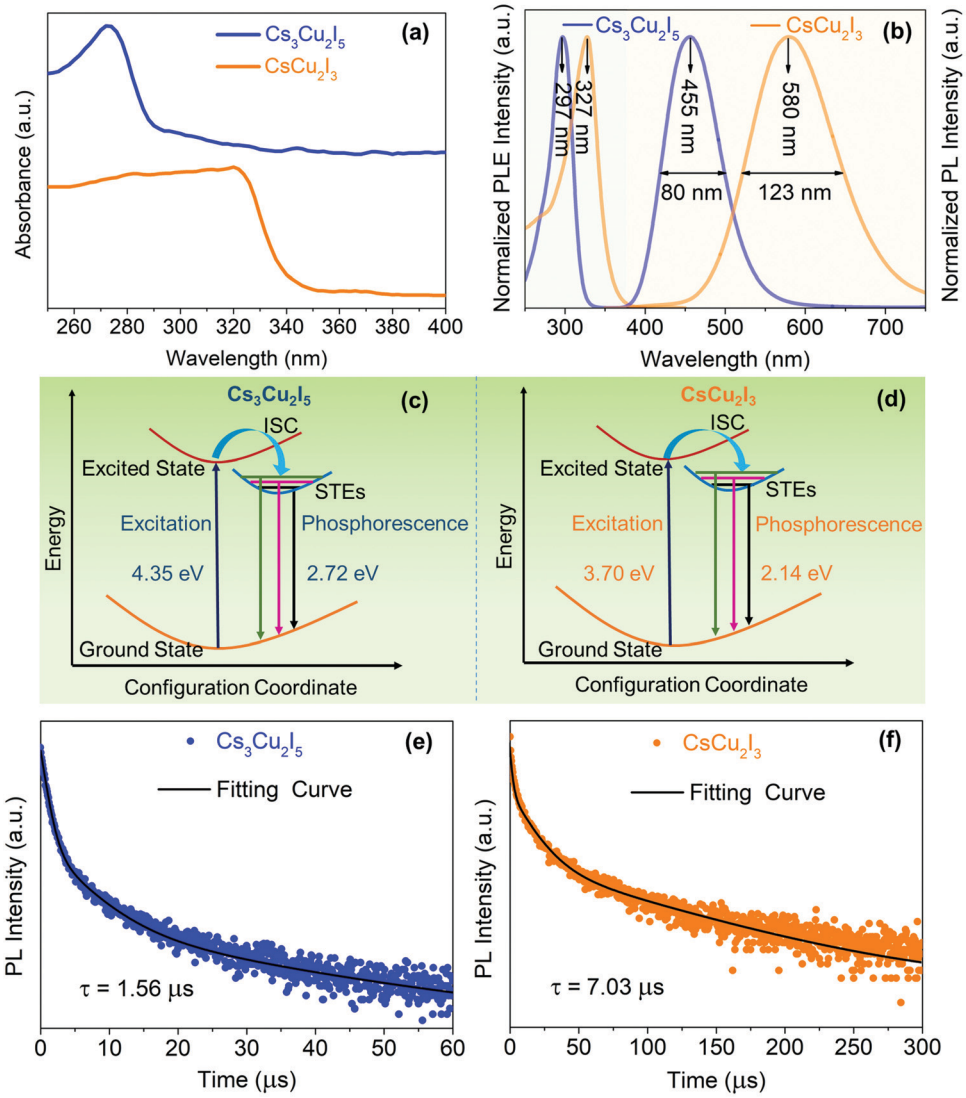

Fig. 3 (a) UV-vis absorption spectra of $Cs_3Cu_2I_5$ and $CsCu_2I_3$. (b) PLE and PL spectra of $Cs_3Cu_2I_5$ and $CsCu_2I_3$. Schematic diagram of the STE emission of (c) $Cs_3Cu_2I_5$ and (d) $CsCu_2I_3$. Time-resolved PL decay spectra of (e) $Cs_3Cu_2I_5$ and (f) $CsCu_2I_3$.

corresponding pseudocolor map of $Cs_3Cu_2I_5$ are shown in Fig. 4(c) and (d). With the increase of temperature, the PL intensity decreases monotonously and the FWHM increases simultaneously, further confirming that a strong electron–phonon coupling results in a highly distorted excited state at high temperatures, so the broadband emission is associated with STE-based radiative recombination. Generally, the temperature-dependent PL intensity can be described by eqn (1):[42]

$$I(T) = \frac{I(0)}{1 + A\exp\left(\frac{-E_b}{k_B T}\right)} \quad (1)$$

where $I(T)$ and $I(0)$ are the integrated PL intensities at a finite temperature and 0 K, respectively. A is a proportional coefficient, and k_B is the Boltzmann constant. E_b, *i.e.*, the exciton binding energy obtained by fitting the curve (Fig. 4(e)) is 285 meV, which is much higher than that of the three-dimensional (3D) LHPs (18 meV),[43] suggesting the unique 0D electronic structure characteristics of $Cs_3Cu_2I_5$.

Moreover, the temperature-dependent FWHM can be described by eqn (2):[21]

$$\mathrm{FWHM}(T) = 2.36\sqrt{s}\hbar\omega_{\mathrm{phonon}}\sqrt{\coth\left(\frac{\hbar\omega_{\mathrm{phonon}}}{2k_B T}\right)} \quad (2)$$

By fitting the curve in Fig. 4(f), the value of the phonon frequency ($\hbar\omega_{\mathrm{phonon}}$) is calculated to be 38 meV, which is comparable to those of LHPs ($\approx$16–40 meV).[13,29,44] It is worthwhile to note that the best fit gives a Huang–Rhys factor (S) value of 33, which is much larger than that of LHPs reported in the literature,[45] and to some extent, it indicates a strong electron–phonon coupling in $Cs_3Cu_2I_5$, thus the STEs can be easily formed.[46]

As a comparison, we also examined the temperature-dependent PL spectra of $CsCu_2I_3$, as shown in Fig. 5(a).

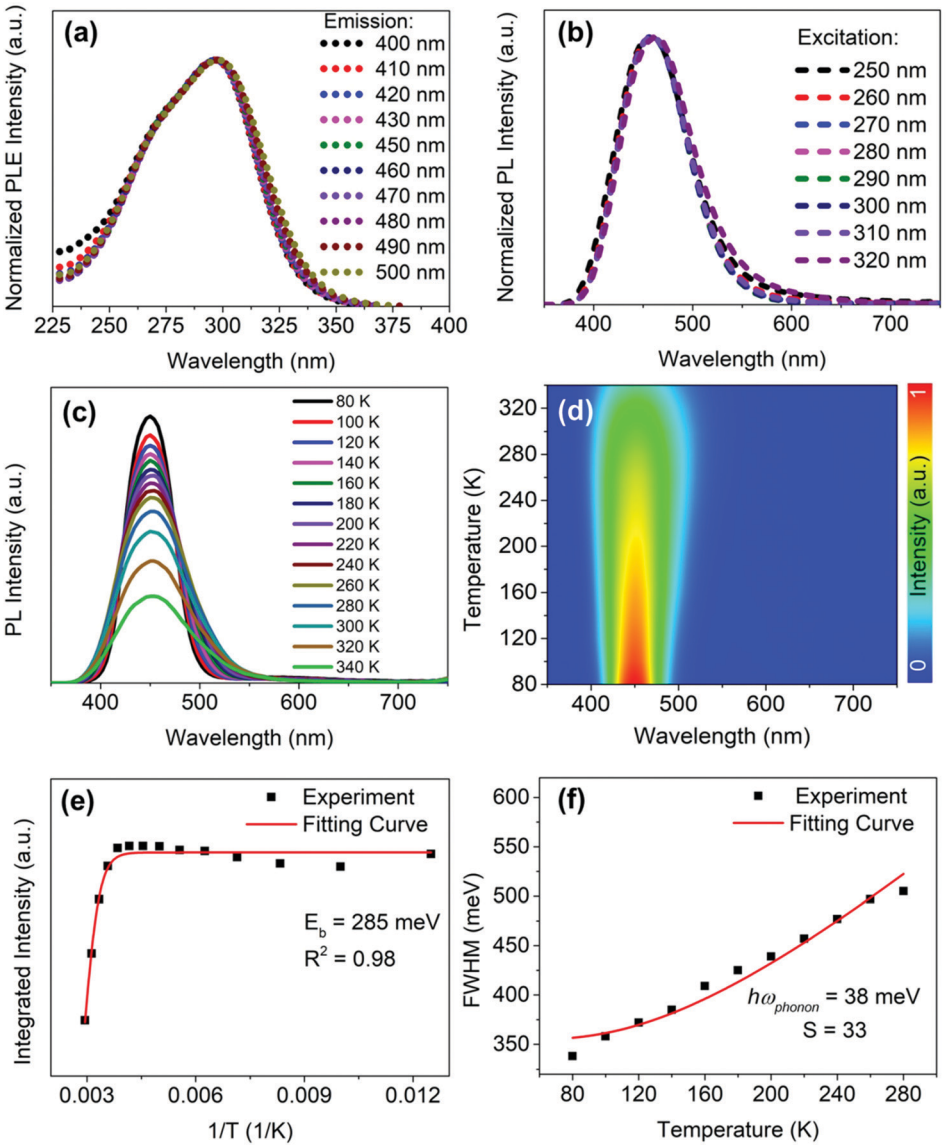

Fig. 4 (a) PLE spectra of $Cs_3Cu_2I_5$ measured at different emission wavelengths. (b) PL spectra of $Cs_3Cu_2I_5$ measured at different excitation wavelengths. (c) Temperature-dependent PL spectra and (d) pseudocolor map of the temperature-dependent PL spectra of $Cs_3Cu_2I_5$. (e) Fitting result of the integrated PL intensity as a function of temperature. (f) Fitting result of the FWHM as a function of temperature.

Interestingly, however, as the temperature increases from 80 K, the PL intensity first decreases rapidly, followed by an increase with further increasing the temperature from 160 to 240 K (see Fig. 5(b)). The temperature-dependent PL intensity of $CsCu_2I_3$ can be well fitted by adopting a combined exciton-trap model as expressed in eqn (3):

$$I(T) = I_0 \frac{1 + C\exp\left(-\frac{E_c}{k_B T}\right)}{1 + A\exp\left(-\frac{E_a}{k_B T}\right) + B\exp\left(-\frac{E_b}{k_B T}\right)} \quad (3)$$

where $I(T)$ and $I(0)$ represent the integrated PL intensities at a finite temperature and 0 K. A, B and C are the fitting parameters, and k_B is the Boltzmann constant. E_a is the self-trapped depth, E_b is the exciton binding energy, and E_c is related to the thermal quenching of the PL intensity. By fitting the curve in Fig. 5(c), the values of E_a, E_b and E_c are 443, 107 and 194 meV, respectively. Similarly, fitting the data by using eqn (2) yield an increasing trend of FWHM for $CsCu_2I_3$, as described in Fig. 5(d). As compared with $Cs_3Cu_2I_5$ ($E_b \approx 285$ meV), the smaller exciton binding energy of $CsCu_2I_3$ ($E_b \approx 107$ meV) would lead to a low radiative recombination rate and the reduced PLQY, which agree well with the results as mentioned earlier.

Taken together, there are two competing processes involved in the evolution of the PL intensity as a function of temperature as follows.

(1) While weaker PL is normally observed at higher temperatures due to the enhanced phonon-assisted nonradiative recombination, which is commonly known as the thermal quenching process. Furthermore, at a lower temperature, the lattice has insufficient

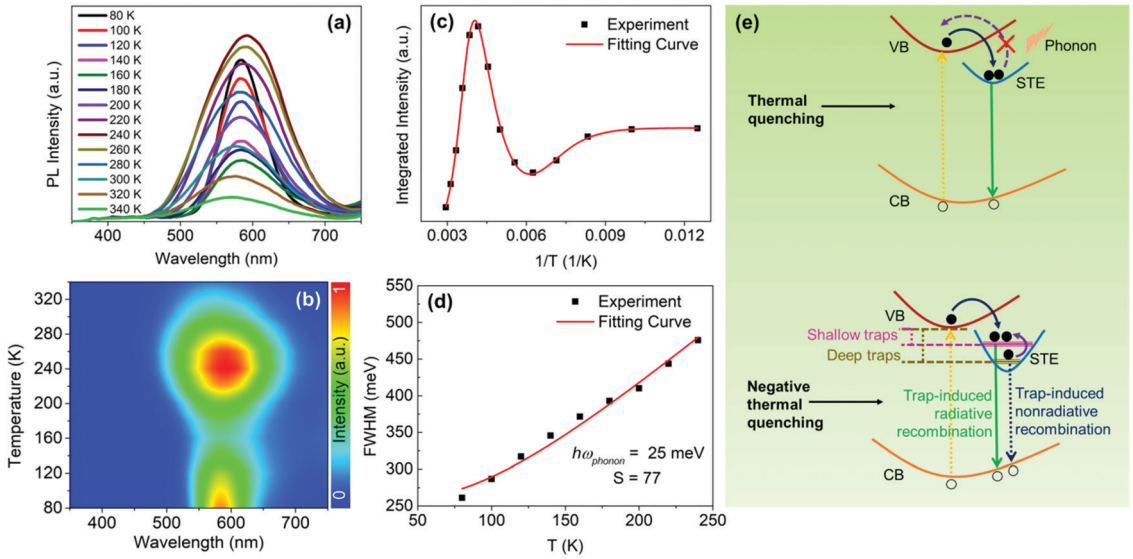

Fig. 5 (a) Temperature-dependent PL spectra and (b) pseudocolor map of the temperature-dependent PL spectra of $CsCu_2I_3$. (c) Fitting result of the integrated PL intensity as a function of temperature. (d) Fitting result of the FWHM as a function of temperature. (e) Schematic diagram of thermal quenching and negative thermal quenching processes.

thermal energy to detrap electrons from STEs to free excitons states.[47] In contrast, at a higher temperature, the thermal energy becomes increasingly sufficient for trapped electrons in the STE state to break through the activation-energy barrier (*i.e.*, self-trapping depth) to detrap, which may result in the decreased population of excitons and the subsequent thermal quenching of STE emission.

(2) The evolution of the temperature-dependent PL intensity can also be affected by a phenomenon designated as negative thermal quenching, in which the PL intensity increases with increasing the temperature.[48] In this work, it is can be ascribed to the thermal excitation of the more deeply trapped nonradiative STE states toward the shallowly trapped radiative STE states,[26] giving an enhancement of the STE emission, as shown in Fig. 5(e).

Here, the evolution trend of the PL intensity of $Cs_3Cu_2I_5$, as a function of temperature is dominated by the thermal quenching behavior (*i.e.*, weaker PL at higher temperatures), which is usually observed and typically expected in semiconductors.[49,50] In contrast, $CsCu_2I_3$ exhibits an unusual trend, distinctly different from the previously reported results.[51] According to the fitting result that the self-trapped depth of $CsCu_2I_3$ ($E_a \approx$ 443 meV) is greatly larger than the thermal perturbation at room temperature ($k_BT \approx$ 26 meV). In brief, we speculate that, at a relatively low temperature, k_BT is not large enough to thermally detrap the trapped electrons back to the conduction band, but rather probably bring the electrons from the deep STE states to the shallow STE states. Therefore, these deeply trapped electrons will decay through a pathway of nonradiative recombination, whereas these shallowly trapped electrons will participate in the radiative recombination, finally resulting in the observed negative thermal quenching (*i.e.*, stronger PL at higher temperatures), which is the dominant process at a temperature range of 160–240 K for $CsCu_2I_3$.

In this work, we could also directly synthesize a series of $Cs_3Cu_2I_5$@$CsCu_2I_3$ composites by a microwave method with changing the amount of CuI. As shown in the inset of Fig. 6(a), the photographs of five powder samples under ambient light and UV lamp (254 nm) display the emission colors of blue, blue-white, white, yellow-white and yellow, respectively. According to the PLE spectra of $Cs_3Cu_2I_5$ and $CsCu_2I_3$ (Fig. S4, ESI†), the overlapped excitation band (270–330 nm) could simultaneously motivate the blue- and yellow-emissive ingredients, yielding the white light. Therefore, 310 nm was chosen as the optimal excitation wavelength to measure the PL spectra of $Cs_3Cu_2I_5$@$CsCu_2I_3$ composites, as shown in Fig. 6(a). It is clearly observed that the pure $Cs_3Cu_2I_5$ synthesized with 1.3 mmol CuI and pure $CsCu_2I_3$ synthesized with 2 mmol CuI display the single-peak emission, while $Cs_3Cu_2I_5$@$CsCu_2I_3$ composites (1.6, 1.7 and 1.8 mmol of CuI) show the double-peak emissions at 455 and 580 nm. Besides, with the increasing amount of CuI, the intensity of the emission peak at 580 nm gradually increases, and the intensity of the emission peak at 455 nm gradually decreases. It is a strong evidence that there is an evolution trend of the two ingredients in the composites, which is consistent with the XRD results. To further verify it, the molar contents of $CsCu_2I_3$ and $Cu_3Cu_2I_5$ in the composites (Table S1, ESI†) are estimated from the quantitative analysis of XRF spectra (Fig. S5, ESI†). Accordingly, the corresponding CIE color coordinates of $Cs_3Cu_2I_5$@$CsCu_2I_3$ composites shift from cold-white light (0.27, 0.27) to warm-white light (0.38, 0.40) respectively, as shown in Fig. 6(b). We also studied the emission of the $Cs_3Cu_2I_5$@$CsCu_2I_3$ composite under different excitation light wavelengths of 305–315 nm (Fig. 6(c)). It is found that the corresponding pseudocolor map (Fig. 6(d)) displays a regular variation tendency, implying a competitive relationship between the two emissive ingredients. Consequently, the CIE color

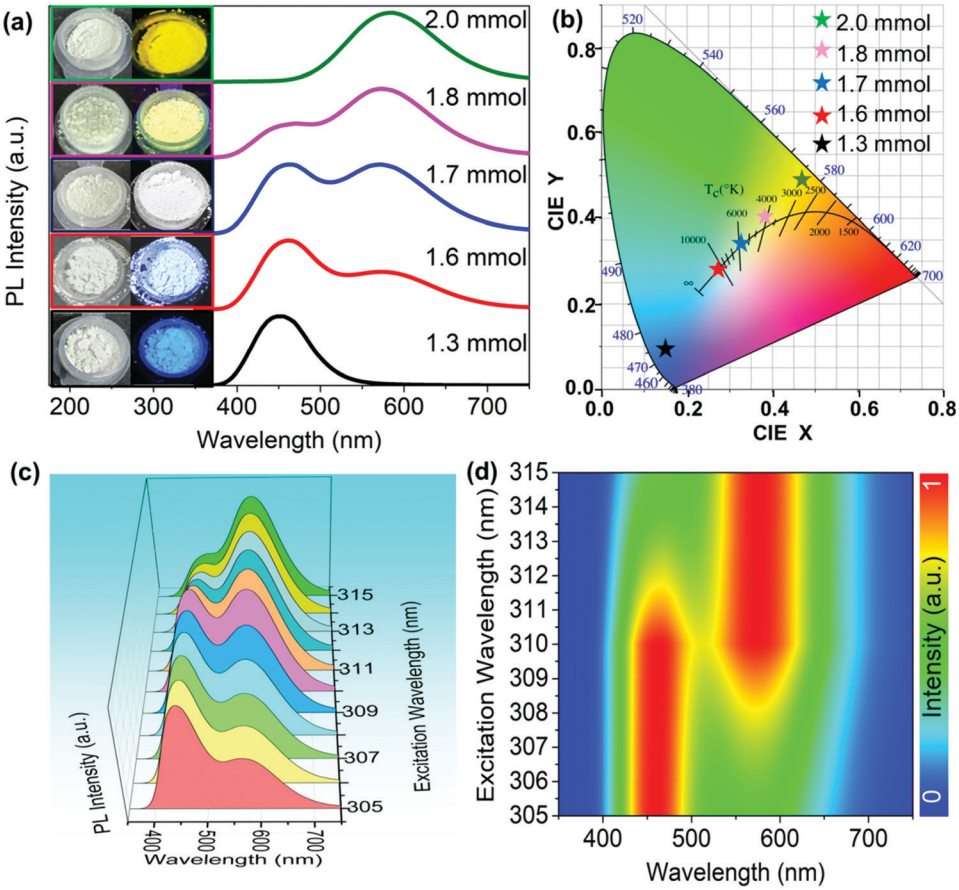

Fig. 6 (a) PL spectra of all samples obtained using an excitation wavelength of 310 nm. The insets are the photographs of powder samples synthesized with different amounts of CuI under ambient light and UV lamp at 254 nm, respectively. (b) Corresponding CIE color coordinates of all samples. (c) PL spectra of the $Cs_3Cu_2I_5$@$CsCu_2I_3$ composite with a CuI amount of 1.7 mmol, obtained using different excitation wavelengths. (d) Pseudocolor map of the PL spectra of the $Cs_3Cu_2I_5$@$CsCu_2I_3$ composite under different excitation wavelengths.

coordinates exhibit a continuous shift from cold-white light (0.27, 0.27) to warm-white light (0.39, 0.41), as shown in Fig. S6 (ESI†), similar to the effect of different addition amounts of CuI.

The above results clarify that the cold/warm white-light tuning stems from the independent blue and yellow light emissions in $Cs_3Cu_2I_5$@$CsCu_2I_3$ composites, which can be achieved by flexibly adjusting the PL intensity ratio for the two ingredients. In addition, the air stability of $Cs_3Cu_2I_5$@$CsCu_2I_3$ composites is evaluated by monitoring XRD and PL (see Fig. S7, ESI†). No additional diffraction peaks were observed in the powder XRD pattern after 80 days, indicating that the samples still maintain the structural integrity. No noticeable degradation of the PL intensity is observed over 60 days exposure under ambient conditions, clarifying that the initial optical performance could be maintained. Such extraordinary air stability makes the $Cs_3Cu_2I_5$@$CsCu_2I_3$ composites display great potential applications in white light illumination.

Herein, three white light devices with different correlated color temperatures (CCT) were fabricated to demonstrate the potential applications of $Cs_3Cu_2I_5$@$CsCu_2I_3$ composites. Fig. 7(a) shows the schematic diagram of the UV pumped WLED devices based on the $Cs_3Cu_2I_5$@$CsCu_2I_3$ composites. The EL spectra of three WLEDs at an operational voltage of 5 V are shown in Fig. 7(b), and the inset photographs display the emission of cold-white (1.6 mmol CuI), pure-white (1.7 mmol CuI) and warm-white (1.8 mmol CuI), respectively. Their corresponding color coordinates and CCT are (0.27, 0.27)/12 810 K, (0.32, 0.33)/6109 K, and (0.38, 0.40)/4149 K, respectively, as shown in Fig. 7(c). A photograph of the working WLED device with an ultra-high CRI of 92 (Fig. 7(d)) displays a good color discrimination. Finally, the operational stability of the WLED (1.7 mmol CuI) operated at a voltage of 5 V under ambient air conditions was investigated. As shown in Fig. S8a and b (ESI†), the WLED can efficiently sustain for 40 h without any emission decay; moreover, CCT and CRI can be maintained for 40 consecutive hours with no obvious change. The current work suggests that the non-toxic $Cs_3Cu_2I_5$@$CsCu_2I_3$ composite with a tunable cold/warm white-light emission should be a promising candidate in the future solid-state lightings.

Conclusions

High-quality copper-based halides with tunable and superior emissive features were successfully synthesized by a microwave

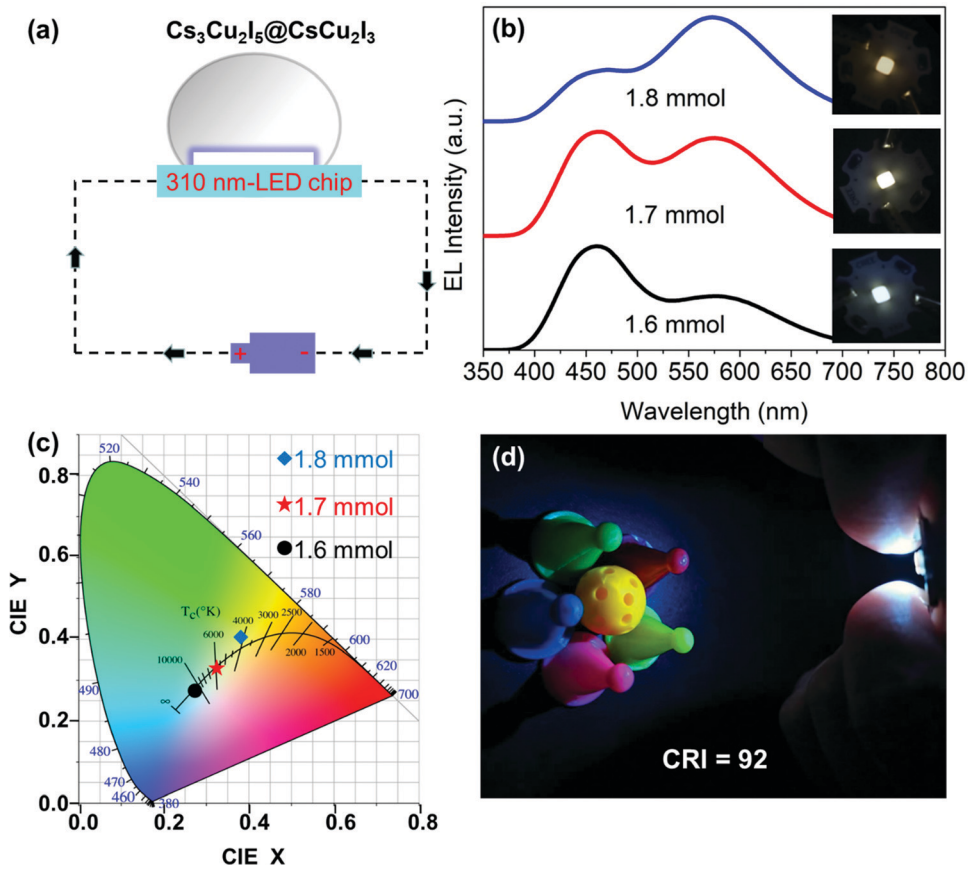

Fig. 7 (a) Schematic diagram of the UV pumped WLED device. (b) EL spectra of the three WLEDs prepared with different amounts of CuI. The insets are the photographs of the devices under an operational voltage of 5 V. (c) CIE color coordinates of the three devices. (d) A typical photograph of the working WLED device with a CRI of 92.

method. It is found that the addition amount of CuI has a great influence on the two broadband emissive materials with STEs, which enables $Cs_3Cu_2I_5$ and $CsCu_2I_3$ to exhibit blue emission (455 nm) with a PLQY of 50% and yellow emission (580 nm) with a PLQY of 9%, respectively, and demonstrate the relatively long lifetimes (1.56 and 7.03 μs), high exciton binding energies (285 and 107 meV) and high electron–phonon coupling factors (33 and 77). Negative thermal quenching owing to the thermal excitation of the more deeply trapped nonradiative STE states toward the shallowly trapped radiative STE states is likely to be responsible for the observed PL enhancement with the increasing temperature. All the findings provide the clear evidence for the formation of STEs, occurring in the material with a strong electron–phonon coupling in the deformable crystal lattice. Furthermore, $Cs_3Cu_2I_5$@$CsCu_2I_3$ composites display the high-quality white emission with cold/warm white-light tuning by changing the addition amount of CuI and the excitation wavelength, together with good air stability. Three WLED devices with CIE color coordinates of (0.27, 0.27), (0.32, 0.33) and (0.38, 0.40) were fabricated using the $Cs_3Cu_2I_5$@$CsCu_2I_3$ composites combined with UV LED chips, and a CRI as high as 92 can be obtained. Together with the feasible processing technique, environmentally friendly properties and cold/warm tunable white light, copper-based halides can thus be regarded as a promising light emitter for the future solid-state lighting technologies.

Conflicts of interest

The authors declare no conflicts of interest.

Acknowledgements

This work was supported by the Natural Science Foundation of Hebei Province (No. A2021201038). The authors acknowledge the Hebei Key Laboratory of Opticelectric Information and Materials, and the National and Local Joint Engineering Laboratory of New Energy Photoelectric Devices for the measurement assistance.

References

1 P. Du, J. Li, L. Wang, L. Sun, X. Wang, X. Xu, L. Yang, J. Pang, W. Liang, J. Luo, Y. Ma and J. Tang, Efficient and large-area all vacuum-deposited perovskite light-emitting diodes *via* spatial confinement, *Nat. Commun.*, 2021, **12**, 4751.

2 Q. S. Hu, G. D. Niu, Z. Zheng, S. R. Li, Y. A. Zhang, H. S. Song, T. Y. Zhai and J. Tang, Tunable color temperatures and efficient white emission from $Cs_2Ag_{1-x}Na_x$-$In_{1-y}Bi_yCl_6$ double perovskite nanocrystals, *Small*, 2019, **15**, 1903496.

3 C. H. Bi, Z. W. Yao, X. J. Sun, X. C. Wei, J. X. Wang and J. J. Tian, Perovskite quantum dots with ultralow trap density by acid etching-driven ligand exchange for high luminance and stable pure-blue light-emitting diodes, *Adv. Mater.*, 2021, **33**, 2006722.

4 Z. Liu, W. D. Qiu, X. M. Peng, G. W. Sun, X. Y. Liu, D. H. Liu, Z. C. Li, F. R. He, C. Y. Shen, Q. Gu, F. L. Ma, L. Yip, L. T. Hou, Z. J. Qi and S. J. Su, Perovskite light-emitting diodes with EQE Exceeding 28% through a synergetic dual-additive strategy for defect passivation and nanostructure regulation, *Adv. Mater.*, 2021, **33**, 2103268.

5 L. Zhu, H. Cao, C. Xue, H. Zhang, M. C. Qin, J. Wang, K. C. Wen, Z. W. Fu, T. Jiang, L. Xu, Y. Zhang, Y. Cao, C. Tu, J. Zhang, D. W. Liu, G. B. Zhang, D. C. Kong, N. Fan, G. Q. Li, C. Yi, Q. M. Peng, J. Chang, X. H. Lu, N. N. Wang, W. Huang and J. P. Wang, Unveiling the additive-assisted oriented growth of perovskite crystallite for high performance light-emitting diodes, *Nat. Commun.*, 2021, **12**, 5081.

6 Y. Shen, H. Y. Wu, Y. Q. Li, K. C. Shen, X. Y. Gao, F. Song and J. X. Tang, Interfacial nucleation seeding for electroluminescent manipulation in blue perovskite light-emitting diodes, *Adv. Funct. Mater.*, 2021, **31**, 2103870.

7 J. Luo, M. Hu, G. Niu and J. Tang, Lead-free halide perovskites and perovskite variants as phosphors toward light-emitting applications, *ACS Appl. Mater. Interfaces*, 2019, **11**, 31575–31584.

8 S. Y. Zhao, W. S. Cai, H. X. Wang, Z. G. Zang and J. Z. Chen, All-inorganic lead-free perovskite(-like) single crystals: Synthesis, properties, and applications, *Small Methods*, 2021, **5**, 2001308.

9 M. G. Ju, J. Dai, L. Ma and X. C. Zeng, Lead-free mixed tin and germanium perovskites for photovoltaic application, *J. Am. Chem. Soc.*, 2017, **139**, 8038–8043.

10 Q. Liu, J. Yin, B. B. Zhang, J. K. Chen, Y. Zhou, L. M. Zhang, L. M. Wang, Q. Zhao, J. Hou, J. Shu, B. Song, N. Shirahata, O. M. Bakr, O. F. Mohammed and H. T. Sun, Theory-guided synthesis of highly luminescent colloidal cesium tin halide perovskite nanocrystals, *J. Am. Chem. Soc.*, 2021, **143**, 5470–5480.

11 C. T. Kang, H. S. Rao, Y. P. Fang, J. J. Zeng, Z. X. Pan and X. H. Zhong, Antioxidative stannous oxalate derived lead-free stable $CsSnX_3$ (X = Cl, Br, and I) perovskite nanocrystals, *Angew. Chem., Int. Ed.*, 2021, **60**, 660–665.

12 Z. Ma, Z. Shi, D. Yang, F. Zhang, S. Li, L. Wang, D. Wu, Y. Zhang, G. Na, L. Zhang, X. Li, Y. Zhang and C. Shan, Electrically-driven violet light-emitting devices based on highly stable lead-free perovskite $Cs_3Sb_2Br_9$ quantum dots, *ACS Energy Lett.*, 2019, **5**, 385–394.

13 J. Zhang, Y. Yang, H. Deng, U. Farooq, X. K. Yang, J. Khan, J. Tang and H. S. Song, High quantum yield blue emission from lead free inorganic antimony halide perovskite colloidal quantum dots, *ACS Nano*, 2017, **11**, 9294–9302.

14 B. Pradhan, G. S. Kumar, S. Sain, A. Dalui, U. K. Ghorai, S. K. Pradhan and S. Acharya, Size tunable cesium antimony chloride perovskite nanowires and nanorods, *Chem. Mater.*, 2018, **30**, 2135–2142.

15 B. Yang, J. S. Chen, F. Hong, X. Mao, K. B. Zheng, S. Q. Yang, Y. J. Li, T. Pullerits, W. Q. Deng and K. L. Han, Lead-free, air-stable all-inorganic cesium bismuth halide perovskite nanocrystals, *Angew. Chem., Int. Ed.*, 2017, **56**, 12471–12475.

16 L. Lian, M. Zheng, P. Zhang, Z. Zheng, K. Du, W. Lei, J. Gao, G. Niu, D. Zhang, T. Zhai, S. Jin, J. Tang, X. Zhang and J. Zhang, Photophysics in $Cs_3Cu_2X_5$ (X = Cl, Br, or I): Highly luminescent self-trapped excitons from local structure symmetrization, *Chem. Mater.*, 2020, **32**, 3462–3468.

17 R. Roccanova, A. Yangui, H. Nhalil, H. Shi, M.-H. Du and B. Saparov, Near-unity photoluminescence quantum yield in blue-emitting $Cs_3Cu_2Br_{5-x}I_x$ ($0 \leq x \leq 5$), *ACS Appl. Electron. Mater.*, 2019, **1**, 269–274.

18 Z. Z. Ma, Z. F. Shi, C. C. Qin, M. H. Cui, D. W. Yang, X. J. Wang, L. T. Wang, X. Z. Ji, X. Chen, J. L. Sun, D. Wu, Y. Zhang, X. J. Li, L. J. Zhang and C. X. Shan, Stable yellow light-emitting devices based on ternary copper halides with broadband emissive self-trapped Excitons, *ACS Nano*, 2020, **14**, 4475–4486.

19 L. T. Wang, Z. Z. Ma, F. Zhang, M. Wang, X. Chen, D. Wu, Y. T. Tian, X. J. Li and Z. F. Shi, Stable down-conversion white light-emitting devices based on highly luminescent copper halides synthesized at room temperature, *J. Mater. Chem. C*, 2021, **9**, 6151–6159.

20 Y. Liu, A. Nag, L. Manna and Z. Xia, Lead-free double perovskite $Cs_2AgInCl_6$, *Angew. Chem., Int. Ed.*, 2021, **60**, 11592–11603.

21 Z. L. Li, Z. H. Rao, Q. Q. Li, L. J. Zhou, X. J. Zhao and X. Gong, $Cs_2Zr_{1-x}Te_xCl_6$ perovskite microcrystals with ultra-high photoluminescence quantum efficiency of 79.46% for high light efficiency white light emitting diodes, *Adv. Opt. Mater.*, 2021, **9**, 2100804.

22 R. Zhang, X. Mao, D. Zheng, Y. Yang, S. Yang and K. Han, A lead-free all-inorganic metal halide with near-unity green luminescence, *Laser Photonics Rev.*, 2020, **14**, 2000027.

23 H. Chen, L. Zhu, C. Xue, P. Liu, X. Du, K. Wen, H. Zhang, L. Xu, C. Xiang, C. Lin, M. Qin, J. Zhang, T. Jiang, C. Yi, L. Cheng, C. Zhang, P. Yang, M. Niu, W. Xu, J. Lai, Y. Cao, J. Chang, H. Tian, Y. Jin, X. Lu, L. Jiang, N. Wang, W. Huang and J. Wang, Efficient and bright warm-white electroluminescence from lead-free metal halides, *Nat. Commun.*, 2021, **12**, 1421.

24 Y. Li, P. Vashishtha, Z. Zhou, Z. Li, S. B. Shivarudraiah, C. Ma, J. Liu, K. S. Wong, H. Su and J. E. Halpert, Room temperature synthesis of stable, printable $Cs_3Cu_2X_5$ (X = I, Br/I, Br, Br/Cl, Cl) colloidal nanocrystals with near-unity quantum yield green emitters (X = Cl), *Chem. Mater.*, 2020, **32**, 5515–5524.

25 P. Sebastia-Luna, J. Navarro-Alapont, M. Sessolo, F. Palazon and H. J. Bolink, Solvent-free synthesis and thin-film deposition of cesium copper halides with bright blue photoluminescence, *Chem. Mater.*, 2019, **31**, 10205–10210.

26 R. Roccanova, A. Yangui, G. Seo, T. D. Creason, Y. Wu, D. Y. Kim, M.-H. Du and B. Saparov, Bright luminescence from nontoxic $CsCu_2X_3$ (X = Cl, Br, I), *ACS Mater. Lett.*, 2019, **1**, 459–465.

27 T. Jun, K. Sim, S. Iimura, M. Sasase, H. Kamioka, J. Kim and H. Hosono, Lead-free highly efficient blue-emitting $cs_3cu_2i_5$ with 0d electronic structure, *Adv. Mater.*, 2018, **30**, 1804547.

28 Z. Luo, Q. Li, L. Zhang, X. Wu, L. Tan, C. Zou, Y. Liu and Z. Quan, 0D $Cs_3Cu_2X_5$ (X = I, Br, and Cl) Nanocrystals: Colloidal syntheses and optical properties, *Small*, 2020, **16**, 1905226.

29 L. Lian, M. Zheng, W. Zhang, L. Yin, X. Du, P. Zhang, X. Zhang, J. Gao, D. Zhang, L. Gao, G. Niu, H. Song, R. Chen, X. Lan, J. Tang and J. Zhang, Efficient and reabsorption-free radioluminescence in $Cs_3Cu_2I_5$ nanocrystals with self-trapped excitons, *Adv. Sci.*, 2020, **7**, 2000195.

30 R. C. Lin, Q. L. Guo, Q. Zhu, Y. M. Zhu, W. Zheng and F. Huang, All-Inorganic $CsCu_2I_3$ single crystal with high-PLQY (approximate to 15.7%) intrinsic white-light emission *via* Strongly localized 1d excitonic recombination, *Adv. Mater.*, 2019, **31**, 1905079.

31 T. D. Creason, A. Yangui, R. Roccanova, A. Strom, M. H. Du and B. Saparov, Rb_2CuX_3 (X = Cl, Br): 1D all-inorganic copper halides with ultrabright blue emission and up-conversion photoluminescence, *Adv. Opt. Mater.*, 2020, **8**, 191338.

32 P. Vashishtha, G. V. Nutan, B. E. Griffith, Y. Fang, D. Giovanni, M. Jagadeeswararao, T. C. Sum, N. Mathews, S. G. Mhaisalkar, J. V. Hanna and T. White, Cesium copper iodide tailored nanoplates and nanorods for blue, yellow, and white emission, *Chem. Mater.*, 2019, **31**, 9003–9011.

33 G. K. Grandhi, N. S.-M. Viswanath, H. B. Cho, J. H. Han, S. M. Kim, S. Choi and W. B. Im, Mechanochemistry as a green route: Synthesis, thermal stability, and postsynthetic reversible phase transformation of highly-luminescent cesium copper halides, *J. Phys. Chem. Lett.*, 2020, **11**, 7723–7729.

34 M. D. Smith and H. I. Karunadasa, White-light emission from layered halide perovskites, *Acc. Chem. Res.*, 2018, **51**, 619–627.

35 X. X. Li, L. C. Zhang, Q. Y. Zheng, Z. Y. Zhou, S. L. He, D. Tian, A. Q. Guo, C. Wang, S. M. Liu, X. B. Chu, C. A.-L. Yang and F. Z. Zhao, Cesium copper iodide perovskite nanoscale-thick films with tunable photoluminescence for white light-emitting diodes, *ACS Appl. Nano Mater.*, 2022, **5**, 917–924.

36 Z. Ma, Z. Shi, D. Yang, Y. Li, F. Zhang, L. Wang, X. Chen, D. Wu, Y. Tian, Y. Zhang, L. Zhang, X. Li and C. Shan, High color-rendering index and stable white light-emitting diodes by assembling two broadband emissive self-trapped excitons, *Adv. Mater.*, 2021, **33**, 2001367.

37 Q. A. Akkerman, G. Raino, M. V. Kovalenko and L. Manna, Genesis, challenges and opportunities for colloidal lead halide perovskite nanocrystals, *Nat. Mater.*, 2018, **17**, 394–405.

38 T. H. Han, S. Tan, J. L. Xue, L. Meng, J. W. Lee and Y. Yang, Interface and defect engineering for metal halide perovskite optoelectronic devices, *Adv. Mater.*, 2019, **31**, 1803515.

39 L. Wang, Z. Shi, Z. Ma, D. Yang, F. Zhang, X. Ji, M. Wang, X. Chen, G. Na, S. Chen, D. Wu, Y. Zhang, X. Li, L. Zhang and C. Shan, Colloidal synthesis of ternary copper halide nanocrystals for high-efficiency deep-blue light-emitting diodes with a half-lifetime above 100 h, *Nano Lett.*, 2020, **20**, 3568–3576.

40 P. Cheng, L. Sun, L. Feng, S. Yang, Y. Yang, D. Zheng, Y. Zhao, Y. Sang, R. Zhang, D. Wei, W. Deng and K. Han, Colloidal synthesis and optical properties of all-inorganic low-dimensional cesium copper halide nanocrystals, *Angew. Chem., Int. Ed.*, 2019, **58**, 16087–16091.

41 G. Seo, H. Jung, T. D. Creason, V. Yeddu, M. Bamidele, E. Echeverria, J. Lee, D. McIlroy, B. Saparov and D. Y. Kim, Lead-free halide light-emitting diodes with external quantum efficiency exceeding 7% using host–dopant strategy, *ACS Energy Lett.*, 2021, **6**, 2584–2593.

42 G. Longo, M. G. La-Placa, M. Sessolo and H. J. Bolink, High photoluminescence quantum yields in organic semiconductor-perovskite composite thin films, *ChemSusChem*, 2017, **10**, 3788–3793.

43 H. Z. Yang, Y. H. Zhang, J. Pan, J. Yin, O. M. Bakr and O. F. Mohammed, Room-temperature engineering of all-inorganic perovskite nanocrsytals with different dimensionalities, *Chem. Mater.*, 2017, **29**, 8978–8982.

44 A. A. Lohar, A. Shinde, R. Gahlaut, A. Sagdeo and S. Mahamuni, Enhanced photoluminescence and stimulated emission in $cspbcl_3$ nanocrystals at low temperature, *J. Phys. Chem. C*, 2018, **122**, 25014–25020.

45 X. Z. Lao, Z. Yang, Z. C. Su, Z. L. Wang, H. G. Ye, M. Q. Wang, X. Yao and S. J. Xu, Luminescence and thermal behaviors of free and trapped excitons in cesium lead halide perovskite nanosheets, *Nanoscale*, 2018, **10**, 9949–9956.

46 J. J. Luo, X. M. Wang, S. R. Li, J. Liu, Y. M. Guo, G. D. Niu, L. Yao, Y. H. Fu, L. Gao, Q. S. Dong, C. Y. Zhao, M. Y. Leng, F. S. Ma, W. X. Liang, L. D. Wang, S. Y. Jin, J. B. Han, L. J. Zhang, J. Etheridge, J. B. Wang, Y. F. Yan, E. H. Sargent and J. Tang, Efficient and stable emission of warm-white light from lead-free halide double perovskites, *Nature*, 2018, **563**, 541–545.

47 Y. C. Ling, L. Tan, X. Wang, Y. Zhou, Y. Xin, B. W. Ma, K. Hanson and H. W. Gao, Composite perovskites of cesium lead bromide for optimized photoluminescence, *J. Phys. Chem. Lett.*, 2017, **8**, 3266–3271.

48 H. Shibata, Negative thermal quenching curves in photoluminescence of solids, *Jpn. J. Appl. Phys.*, 1998, 550–553.

49 Y. M. Zhao, C. Riemersma, F. Pietra, R. Koole, C. D. Donega and A. Meijerink, High-temperature luminescence quenching of colloidal quantum dots, *ACS Nano*, 2012, **6**, 9058–9067.

50 Z. Tan, Y. Chu, J. Chen, J. Li, G. Ji, G. Niu, L. Gao, Z. Xiao and J. Tang, Lead-free perovskite variant solid solutions $Cs_2Sn_{1-x}Te_xCl_6$: Bright luminescence and high anti-water stability, *Adv. Mater.*, 2020, **32**, 2002443.

51 R. Lin, Q. Zhu, Q. Guo, Y. Zhu, W. Zheng and F. Huang, Dual self-trapped exciton emission with ultrahigh photoluminescence quantum yield in $CsCu_2I_3$ and $Cs_3Cu_2I_5$ perovskite single crystals, *J. Phys. Chem. C*, 2020, **124**, 20469–20476.